High-altitude testing of parachutes; a low-cost methodology for parachute evaluation using consumer electronics

Iain C. Waugh,* Edward A. Moore,* Daniel G. T. Strange,* John Cormack* and Fergus Noble*

CUSF, University of Cambridge, Cambs., CB2 1PZ, United Kingdom

John C. Underwood†

Vorticity Ltd, Chalgrove, Oxfordshire, OX44 7RW, United Kingdom

This paper presents a low-cost method for testing the inflation behaviour of small ($<$ 5m) parachutes at high-altitude and high subsonic Mach numbers. A small and light drop vehicle (11.7kg) was developed and used to test a 2.55m ringslot parachute at a velocity of 210.5m/s (Mach 0.71), an altitude of 22.2km (72,800ft) and an atmospheric density of 0.056kg/m^3. Sensors and cameras mass-produced for consumer electronics are used in a custom avionics package because they are small, low-cost, lightweight and low power. Acceleration, rotation rate and dynamic pressure data are recorded at 2kHz, and high-speed video at 300fps, during inflation and descent. The per-launch expendable costs (balloon, helium etc.) are of the order of several thousand pounds (GBP). This provides an extremely cost effective way of testing small parachutes for stability and performance at the design Mach number and appropriate mass ratio.

I. Introduction

This paper describes a low-cost method for the experimental verification of parachutes designed for low-density, high-speed deployment, such as those required for planetary entry or sample return. There are various methods for evaluating parachutes in these regimes, but there are few physical test data that match both the mass ratios and dynamic pressures for deployment at the required Mach numbers.

The available test data in the literature stem mostly from four NASA programmes completed in the 1960s; namely the Planetary Entry Parachute Program[1–3] (PEPP), the Supersonic Planetary Entry Decelerator Program[4] (SPED-I), the Supersonic High Altitude Parachute Experiment[5] (SHAPE) and the Balloon Launched Decelerator Tests (BLDT). The results from these tests are summarised in Cruz and Lingard[6]. There are some additional data available from the successful descents of recent planetary probes, although appropriate instrumentation on the crafts was limited. The data from the NASA tests span Mach numbers of 1.16 to 3.31, for several parachute configurations (disk gap-band, cruciform and ring sail).

The NASA tests demonstrated that the opening performance of such parachutes is strongly dependent on Mach number, particularly in the transient behaviour following deployment. Due to the costs associated with the NASA programmes only 16 tests were completed, so additional experimental data are required to verify the effects of scaling and Mach number on high-speed parachute performance.

More recently, the high-altitude test program for a Mars Subsonic Parachute[7] (MSP) used a balloon lofted vehicle to evaluate the inflation characteristics of a 33.5m ringsail parachute. For these subsonic tests, rocket boosters were not necessary; the vehicle was simply lofted to 36km and dropped. This method is cost-effective for subsonic tests, in that the mission costs were of the order of several hundred thousand dollars rather than several million dollars for the NASA PEPP tests. A similar method is presented in this paper, at a smaller scale, with mission costs of the order of several thousand dollars.

The MSP high-altitude tests highlighted several design inadequacies that were not identified with low-altitude tests, due to the difference in inflation conditions. For parachute testing to be representative,

*Student, AIAA Student Member.
†Principal Engineer, AIAA Senior Member.

inflation must be at the design Mach number, appropriate mass ratio and scale. This paper aims to provide a low-cost method for testing small parachutes (< 5m) with the first two of these criteria; Mach number and appropriate mass ratio. Only limited testing has taken place in these conditions. It is hoped that an easily repeatable, low-cost testing method will increase knowledge in this area and provide a useful method of evaluating initial designs for large planetary entry projects.

The parachute deployment requirements for this project, and the final drop vehicle measurements, are shown in Tables 1 and 2. The test parachute is a 1/10th scale model of the original second parachute in the ExoMars parachute system, as used in the wind tunnel tests of Lingard et al[10]. The drop vehicle design is relatively small and light, due to the use of a small test parachute and the development of a compact avionics package. The avionics package uses sensors and cameras mass-produced for consumer electronics, because they are small, lightweight and low power, as well as being much more cost-effective than industry standard packages. With a light drop vehicle (11.7kg), off-the-shelf weather balloons can be used to achieve the desired altitudes. Latex weather balloons are much less complex to launch than zero-pressure balloons, and are extremely low-cost for their performance. The balloon used in this project cost only £300 (GBP).

Mach	0.8
Altitude	21.5km
Density	0.069kg/m^3
Type	Ringslot
Diameter	2.55m
Geometric porosity	20%
Predicted Inflation force	5.5kN

Table 1. Parachute deployment requirements.

Body diameter	0.19m
Length	1.40m
Fin span	0.89m
Packed weight	11.7kg
Reserve parachute	72” Cruciform
Abort parachute	15ft Flat Circular
Spring pilots	36” Spring Drogue

Table 2. Final drop vehicle measurements.

The focus of this paper is to present a low-cost method for testing small (< 5m) parachutes at high Mach numbers in low density environments. The paper will first cover the flight profile of the vehicle in the standard and failure cases. The paper will then cover the mechanical design of the drop vehicle, the design of the avionics package, and the low-altitude and high-altitude testing of the subsystems. The paper ends with the results of the test parachute inflation at a velocity of 210.5m/s (Mach 0.71) and an altitude of 22.2km (72,800ft). The results are discussed briefly, but full stability analysis of the test parachute is not included as this is not the focus of this paper.

II. Flight Profile

In the standard case the drop vehicle is lifted by a latex weather balloon to above 24.5km. During ascent, the vehicle hangs from a 15ft predeployed abort parachute. When the vehicle reaches the correct altitude, system safety checks are performed and the test is initiated remotely via radio command. The vehicle cuts away from the balloon using a pyrotechnic device and freefalls for 23s to achieve the required deployment Mach number. A spring pilot parachute is then ejected from the rear of the vehicle, deploying the test parachute from its deployment bag. The vehicle then descends under the test parachute until 200m altitude, where it separates into two halves to reduce landing momentum. The rear half lands under the test parachute and the nosecone half lands under the backup parachute. Sensor data and high-speed video are recorded during inflation and descent.

Emphasis was placed on designing a system with failsafes, and the failure case flight profiles are considered in Figure 2. If the flight must be aborted, an abort command can be sent via radio to either of two flight computers. Both flight computers control a separate pyrotechnic device that cuts away from the balloon, so that the vehicle descends under the predeployed abort parachute. In the case of premature balloon burst, the vehicle would descend under the predeployed abort parachute, with the option of cutting away balloon remnants when descent is detected. In the event of both flight computers failing, the balloon would ascend until it burst, before descending under the abort parachute.

A second failure case is where the test parachute fails to deploy correctly, due to an electrical or mechanical fault, or damage to the parachute during inflation. In this case, either of the two flight computers can deploy the backup parachute. The backup parachute is packed in the nosecone half of the vehicle, so the vehicle

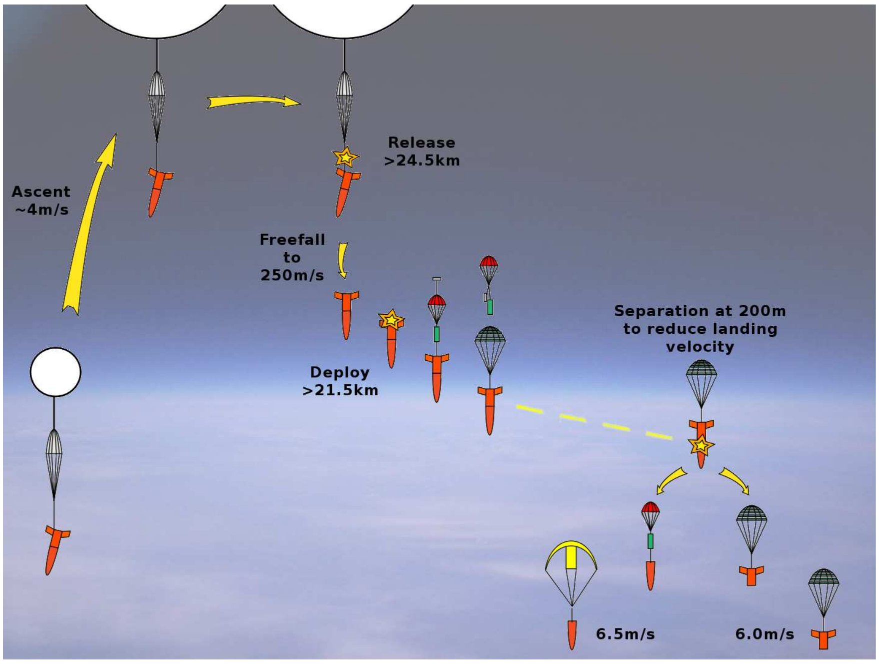

Figure 1. Standard flight profile: (1) Vehicle ascends to test altitude, (2) Drop sequence initiated via radio uplink command, (3) Sensor safety checks performed, backup parachute timer armed and camera started, (4) Vehicle is released from the balloon with a pyrotechnic device and freefalls for 23s, (5) Test parachute is deployed with a spring pilot parachute, (6) Sensor checks performed to assure the parachute has deployed correctly and the backup parachute timer disarmed (Backup parachute deployed if checks are failed), (7) At 200m (or uplink command) the inter-stage tether is released and the vehicle separated. The two stages land separately to reduce landing momentum.

splits with a pyrotechnically activated mechanism to release the backup parachute. The two halves of the vehicle are held together in this case by a nylon tether. The backup parachute is a 72” cruciform design that can withstand inflation at high dynamic pressure.

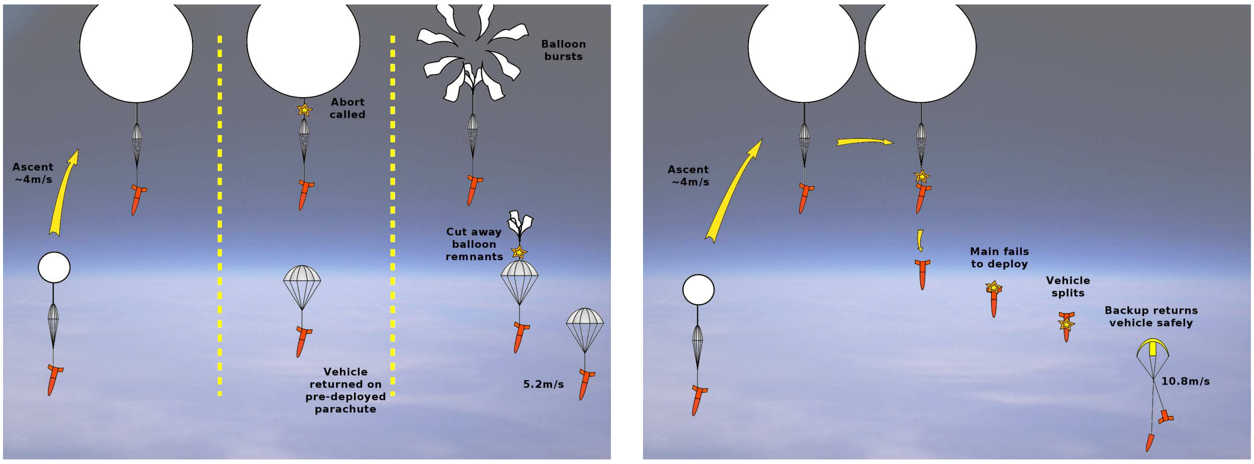

(a) (b)

Figure 2. Failure case flight profiles: (a) If the flight needs to be aborted, or the balloon bursts, the vehicle descends under a 15ft predeployed abort parachute. (b) If the test parachute fails to deploy at test altitude and speed, the vehicle splits and the backup parachute deployed.

III. Vehicle Design - Mechanical

A schematic of the vehicle is shown in Figure 3. The vehicle contains two parachutes: the test parachute in the rear of the vehicle, and the backup parachute in the nosecone of the vehicle. Both of these parachutes are packed in deployment bags and pulled from the vehicle using 36" spring pilot parachutes.

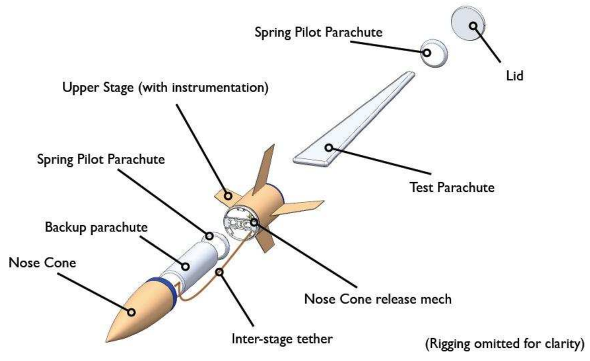

(a) Vehicle schematic

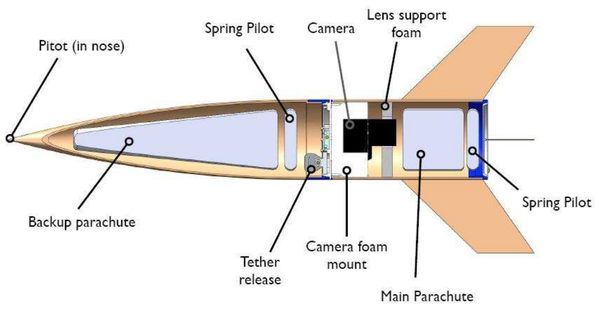

(b) Vehicle cross section

Figure 3. Mechanical design of the drop vehicle. The vehicle is divided into two separable parts; a rear section and a nosecone section. The test parachute is deployed by releasing an aluminium lid from the rear of the vehicle. A spring pilot parachute pulls the test parachute from its deployment bag. The inflation is recorded by a shock mounted high speed camera in the rear of the vehicle. The nosecone section contains another spring pilot parachute to release a backup parachute, which is used in two cases: (1) Test parachute failure, (2) To reduce the landing momentum of the vehicle, the vehicle parts are separated after the test parachute has deployed. The nosecone then lands under the backup parachute. In case (1) the two parts of the vehicle are held together by an inter-stage tether, in case (2) the tether is released with a pyrotechnic mechanism.

In the standard flight profile, the test parachute is ejected rearwards. In the packed configuration the compressed spring pilot parachute is restrained by an aluminium lid at the rear of the vehicle. The aluminium lid is in turn restrained by a nylon shear bolt, which is sheared by two (parallel) Metron DR2006/1 pyrotechnic protractors to eject the parachute. The braided Kevlar bridle is connected directly to a load bearing bulkhead at the centre of the vehicle. The backward facing high-speed camera is housed in the rear of the vehicle, with a foam mounting to reduce shock loads upon parachute inflation.

If either of the flight computers detects that the test parachute has failed to deploy correctly, the backup parachute is deployed. The vehicle is separated at the back of the nosecone using a pyrotechnically activated release mechanism, and a spring pilot parachute pulls the backup parachute from the vehicle. The two halves of the vehicle are connected by an inter-stage tether to the backup parachute.

The backup parachute is also used in the standard flight profile when close to the ground to reduce landing momentum. The vehicle is allowed to descend under the test parachute to ≈ 200m, and then the inter-stage tether is released by a pyrotechnic mechanism within the vehicle. The nosecone section is then released, and the rear and nosecone sections land separately under the test and backup parachutes respectively.

IV. Vehicle Design - Avionics

There are two flight computers in the vehicle; a main flight computer and a backup flight computer. The main flight computer has primary control during the test and interfaces with all sensors. The backup flight computer acts as a reserve for all important flight features, such as receiving radio commands, aborting the mission, or deploying the backup parachute if the test parachute fails to deploy. In this section the key features of the avionics design are described and the failsafe features of the test procedure highlighted.

The main external connections of the flight computers are shown in Figure 4. The main flight computer is mounted on the central load bearing bulkhead; the backup flight computer is mounted at the tip of the nosecone, along with a pitot tube and pressure sensors. Each flight computer has a separate power supply of lithium-ion primary cells. The main flight computer has sole control of the key pyrotechnic devices for the standard drop test: to release from the balloon, to deploy the test parachute and to release the inter-stage tether. Both flight computers control separate pyrotechnic devices for the failure cases: to abort the mission and descend on the abort parachute, or to separate the vehicle and deploy the backup parachute. Because the flight computers and pyrotechnic devices are completely separate, there must be two unconnected system errors before the vehicle would enter into an unplanned flight profile. The vehicle halves must separate so electrical connections between the two halves have inbuilt disconnects.

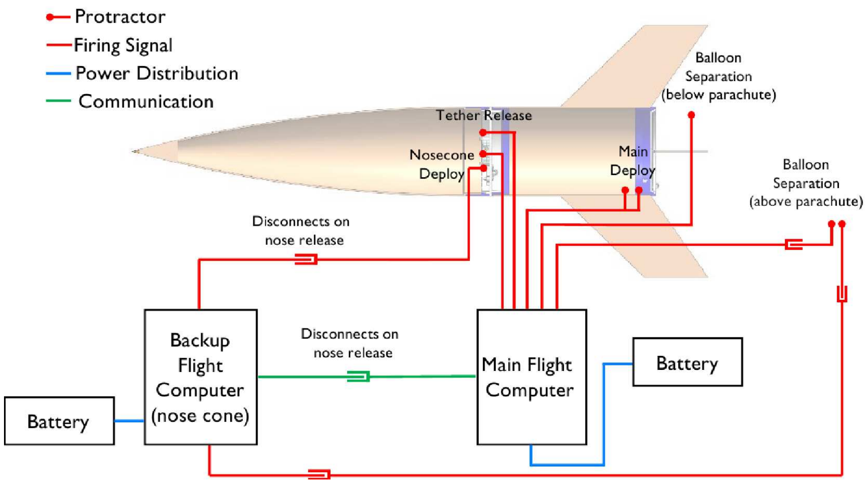

Figure 4. Avionics location and connections to pyrotechnic devices. The main flight computer is located in the rear half of the vehicle. It has sole control of the pyrotechnic devices required for: (1) Balloon separation below the abort parachute to begin freefall, (2) Test parachute deployment (2 parallel devices), (3) Inter-stage tether release for vehicle to land in separate halves. The backup flight computer is located at the tip of the nosecone. Both the main and backup flight computers control separate pyrotechnic devices for: (1) Balloon separation above the abort parachute for mission abort, (2) Nosecone release to separate stages and deploy the backup parachute.

When the vehicle reaches the correct altitude, the standard test procedure is as follows:

1. The electrical continuity of all pyrotechnic devices is checked.
2. The output of all sensors used for deployment logic is checked.
3. If all checks are correct, and the predicted landing locations acceptable, an encoded radio command is sent to the main flight computer to begin the test. The main and backup flight computers use different radio frequencies, and all commands use checksums to avoid false command recognition.
4. The main flight computer checks that the backup flight computer is functioning and connected.
5. The backup parachute deployment timer is set for 26s and initiated on the backup flight computer. The vehicle freefalls for 23s as this is the predicted time required to reach Mach 0.8. The timer will be disabled once the main flight computer detects sufficient deceleration for a correct test parachute deployment. There is a 3s window for this to occur. If contact with the main flight computer is lost, the backup computer automatically deploys the backup parachute after 26s.
6. The main flight computer begins high-speed data logging and video capture.
7. The main flight computer separates from the balloon and abort parachute using a pyrotechnic device, and freefalls for 23s.
8. At 23s, the main flight computer checks the sensors to make sure separation from the balloon was successful.
9. The main flight computer fires the two parallel pyrotechnic protractors at the rear of the vehicle to release the aluminium lid and deploy the spring pilot parachute and test parachute.
10. The main flight computer checks the sensors to ensure the test parachute has deployed and the correct deceleration achieved.
11. The main flight computer disables the backup timer on the backup flight computer.
12. High-speed data and video are recorded at 2kHz onto SD cards during the rest of the vehicle descent.
13. Once enabled by an additional radio command, at 200m the main flight computer releases the inter-stage tether and separates the vehicle to land in two halves. The altitude of the separation can also be altered during the flight to change the landing location.
14. The rear and nosecone halves of the vehicle are tracked separately until landing.

A block diagram of the main flight computer is shown in Figure 5, along with a block diagram of the expansion board that interfaces with the sensors. The modular design allows the avionics package to be easily adapted to use different sensors. The sensor data are read at 2kHz from a serial peripheral interface bus (SPI), and recorded onto an SD card in FAT32 format using direct memory access (DMA) for speed. The radio communications to the ground (uplink and downlink) are handled by the TI CC1111 radio modem microchip. To obey local frequency band regulations, radio power is limited to 10mW, so a low data rate of 50baud is used. During balloon launches for initial subsystem testing, this was found to be sufficient at horizontal ranges up to 200km.

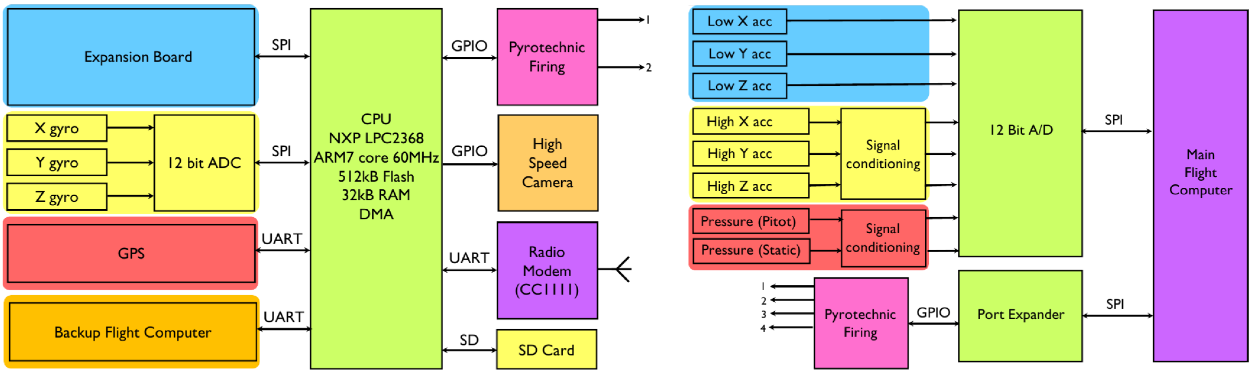

(a) Main flight computer schematic

(b) Expansion board schematic

Figure 5. Block diagram of the avionics design. The main flight computer samples the sensors at 2kHz via a serial peripheral interface (SPI) connection to the sensor board, and logs data with direct memory access (DMA) to a micro SD card in FAT32 format. Radio communications to the ground (uplink and downlink) are handled by the CC1111 radio modem chip.

The key sensors and microchips chosen for the custom avionics are shown in Table 3. All of the components, except the high-range accelerometer, pressure sensors and camera, are small surface mount microchips. The recent drive for high-performance in consumer electronics has increased the accuracy and decreased the size and cost of sensors available. This allows a much smaller and more advanced instrumentation package than was available for the original NASA PEPP tests, and allows high-altitude testing to be carried out for much lower cost. In terms of cost, the only sensor more expensive than a few tens of pounds (GBP) was the high-range piezo accelerometer, which is now within the capability of MEMS devices. The total material cost of the avionics package is roughly £1900, but this is dominated by the cost of the high-range accelerometer (≈£1000) and the high-speed camera (≈£600).

Measurement	Sensor	Range	Accuracy
Position and Velocity	uBlox LEA-5T GPS	-	±10m
Acceleration (3-axis)	Kistler 8792A100	±100g	±1.3g
Acceleration (3-axis)	Freescale MMA7260QT	±6g	±0.06g
Rate Gyroscopes (3-axis)	Invensense IDG650/ISZ650	$\pm 400^o$/s or $\pm 2200^o$/s	$\pm 8^o$/s
Static Pressure	Omegadyne PXM219	0-100kPa absolute	±350Pa
Differential Pressure (pitot)	Honeywell 26PCAFQA1D	0-6.9kPa	±3Pa
Camera	Casio EX-F1	300fps	512x384
Microcontroller	LPC2318 ARM7 core	60MHz	-
Radio Modem	TI CC1111	434.525MHz	-

Table 3. Sensor and chip choices, ranges and accuracies (post filtering and ADC).

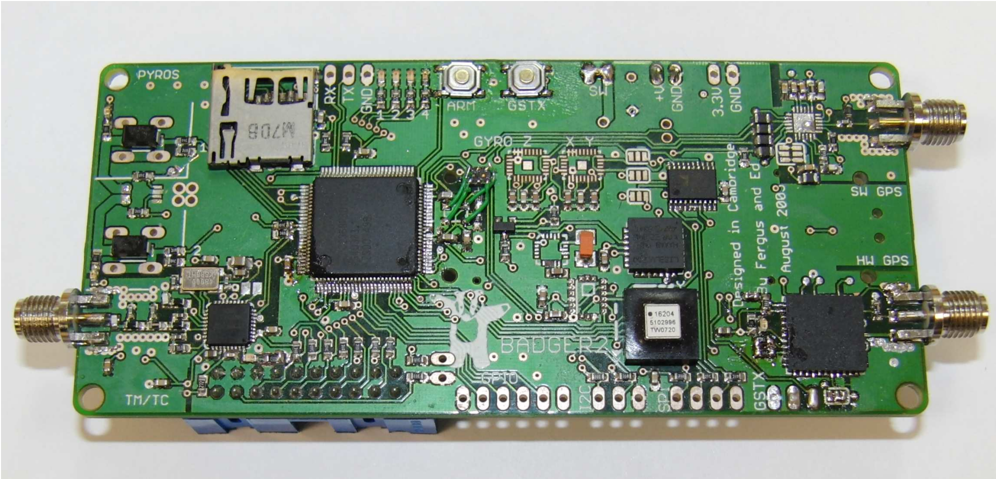

Figure 6. Main flight computer circuit board (115mm x 48mm). The custom main flight computer is based on a 60MHz ARM7 core LPC2368 microchip, CC1111 radio modem, uBlox LEA-5T GPS module and AD7927 12-bit ADC interface to the sensors.

V. Subsystem Testing

This section covers the methods used to test the key drop vehicle subsystems: the avionics, the test parachute deployment mechanism and the backup parachute deployment mechanism.

To test the avionics package at high-altitude conditions, a simplified version of the rear half of the vehicle was launched to 24km under a predeployed parachute. At test altitude the drop was initiated via radio command and the test parachute deployed with a static line. The sensors were shown to give good data throughout the flight and steady state drag data were obtained over a wide density range. The camera footage showed good contrast against the backdrop, both at high and low-altitude (Figure 7). Due to the low loading on the parachute, not all lines were pulled taut on inflation, as can be seen in Figure 7(b). During the ascent, radio uplink and downlink were maintained and tested for signal strength.

The test parachute deployment mechanism was evaluated by attaching the rear half of the vehicle to a trailer towed by a truck, and deploying the parachute at 40mph on an airstrip. High-speed footage was recorded by a chase car (Figure 8), and from the internal camera (Figure 9). The parachute deployment was

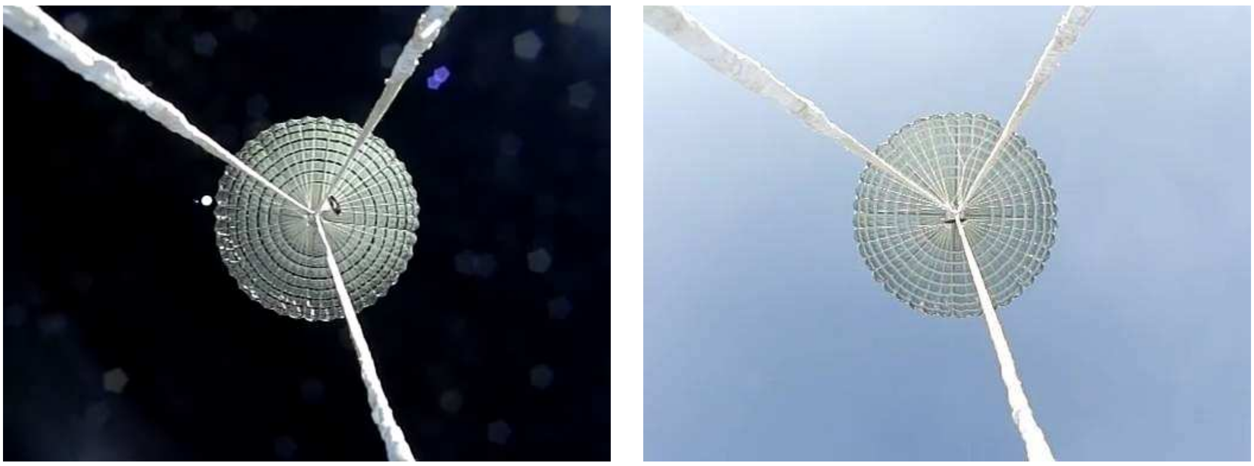

(a) 24km (b) 3.4km

Figure 7. High-speed images of the parachute during the low-speed test. The test parachute is deployed with a static line. The balloon and abort parachute are visible in the background of (a).

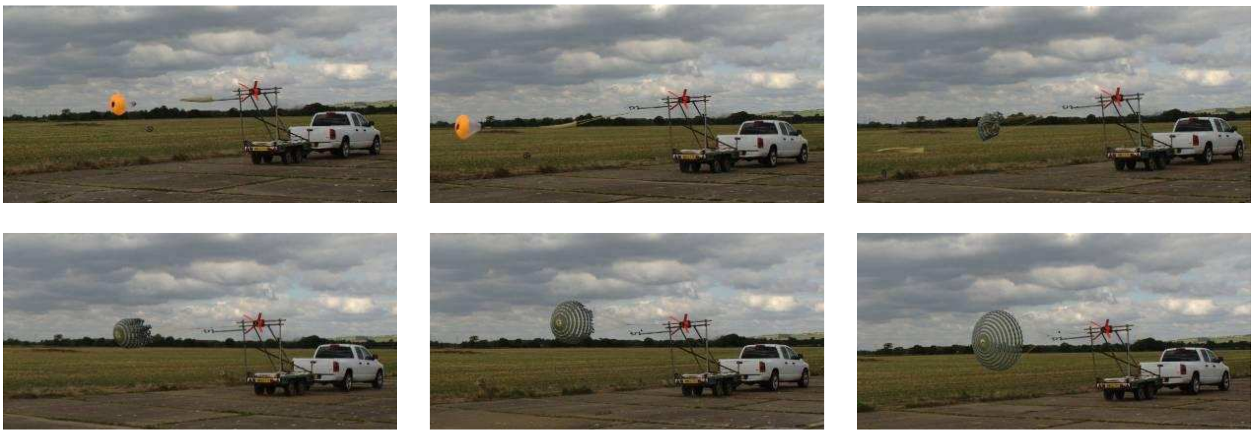

Figure 8. The parachute deployment mechanism is tested at 40mph using the rear half of the drop vehicle mounted on the back of a truck.

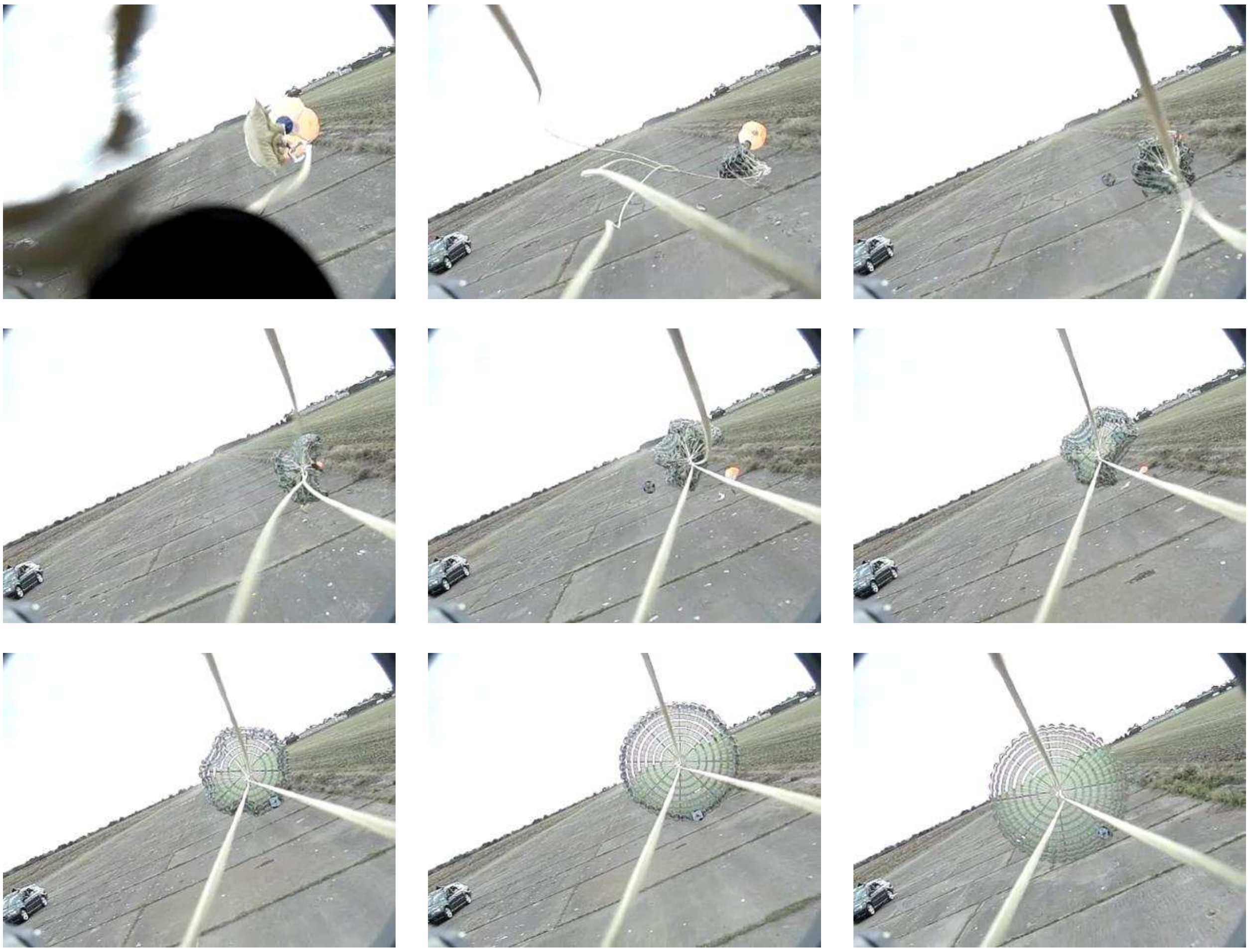

Figure 9. Internal camera recording of the test deployment from the a trailer towed by a truck (see Figure 8) at similar dynamic pressure required for the high-altitude test. The pilot parachute initially deploys towards the right of the frame due to crosswinds on the airstrip. The selected high-speed images (300fps) capture the inflation process.

Figure 10. Low-altitude testing of the standard flight sequence: (1) The vehicle drop is initiated at 1000ft via radio command, (2) The lid and pilot parachute are deployed after 3s freefall (23s for high-altitude drop), (3) Test parachute inflation, (4) Stage separation tether released inside the vehicle, (5) Vehicle separation (at 200m for high-altitude drop), (6) Nose section descends separately under the backup parachute. The inter-stage tether is visible dangling from the nose section.

successful and the internal camera footage sufficient to evaluate the inflation characteristics.

The backup parachute deployment mechanism was tested by dropping the vehicle from a helicopter at 1000ft, as shown in Figure 10. The vehicle then performed a shortened version of the standard flight sequence, containing all key actions: initiation by radio command, pyrotechnic cutaway, timed descent, test parachute deployment, inter-stage tether release, vehicle separation and backup parachute deployment. All actions were successful.

VI. Results

The vehicle drop was initiated at 24.7km, and test parachute inflation occurred 23.8s later at a velocity of 210.5m/s (Mach 0.71), an altitude of 22.2km (72,800ft) and an atmospheric density of 0.056kg/m^3. This is slightly below the design deployment speed of Mach 0.8, due to a higher than expected drag coefficient on the descent. This higher drag coefficient resulted from initial oscillation, before the fins stabilised the descent direction. The standard flight sequence of Figure 1 was followed correctly. Radio downlink was maintained with both flight computers throughout the flight, enabling fast tracking and recovery. The signal strength of the radio link was, however, affected by the rotating of the balloon during ascent, due to the non-uniform radiation pattern of the antenna. The vehicle hangs from the balloon from one attachment point on the side of the vehicle, and thus hangs at an angle of $\approx 13^o$ to the vertical as seen in Figure 1. The rotation of the

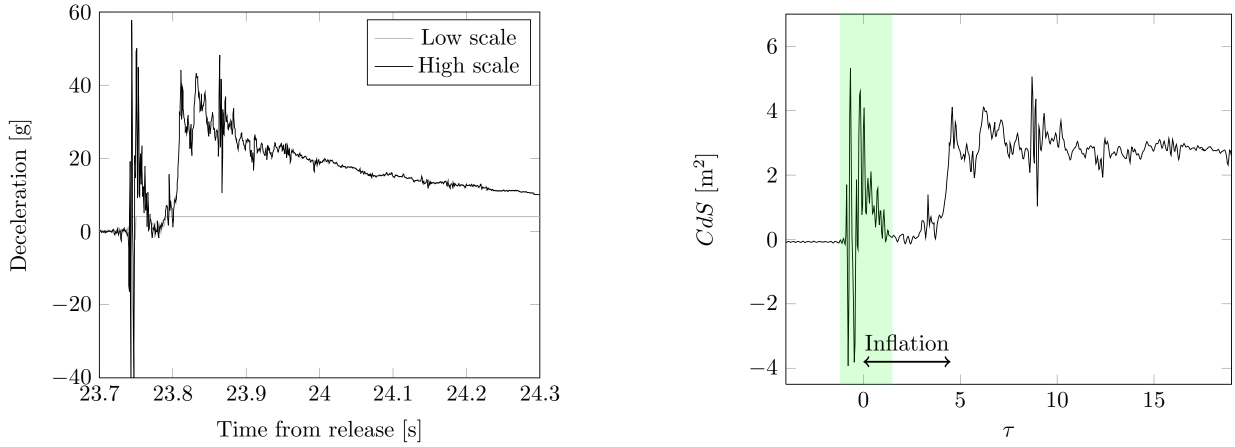

(a)

(b)

Figure 11. Deceleration profile with deployment at a velocity of 210.5m/s (Mach 0.71), an altitude of 22.2km (72,800ft) and an atmospheric density of 0.056kg/m^3, measured using a low scale accelerometer (±6g) and a high scale accelerometer (±100g). The deceleration against time from release is shown in (a), and the drag area, CdS, is plotted against a dimensionless time parameter, τ in (b). The snatch loads are highlighted in green.

balloon swept out a cone with the antenna, modulating the signal strength towards the ground station. It is recommended that the vehicle be hung vertically for future launches.

The deceleration data are shown in Figure 11(a) against time from release, and the drag-area data are shown in Figure 11(b) against dimensionless time. Dimensionless inflation time, τ, is calculated as $\tau = \frac{\mathrm{tV}}{\mathrm{D_0}}$ where t is the real inflation time, $\mathrm{D_0}$ is the parachute reference diameter and V is the initial velocity at the start of inflation.

The data show initially high snatch loads (highlighted in green in Figure 11(b)), followed by a delay as the parachute rebounded. This rebounding is corroborated by the high-speed video in Figure 13. The drag force rapidly increases as the lines become taut and then decreases as the vehicle decelerates. The snatch force follows a triangular profile. The parachute was extracted from the bag at roughly 50m/s, leading to high snatch loads. In order to reduce these loads a smaller pilot parachute is recommended for future tests. The low-scale acceleration sensor is saturated for most of the inflation, but shows good agreement with the high-scale sensor during the rebound period (Figure 11(a)).

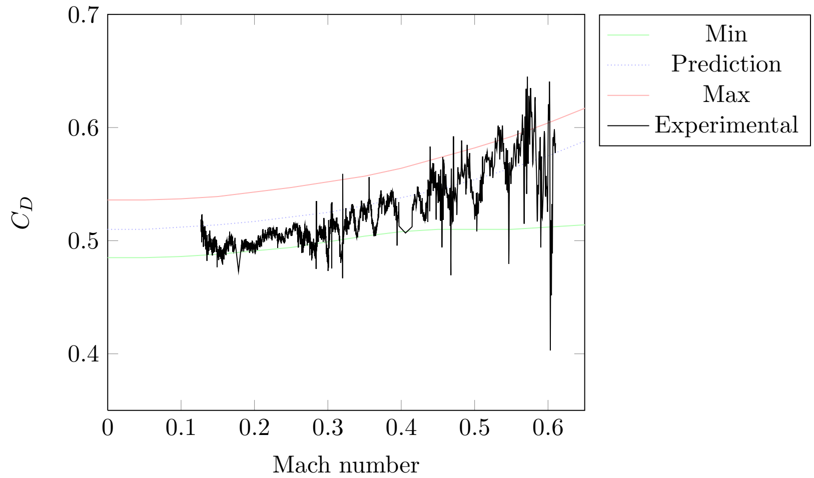

Figure 12. Drag coefficient against Mach number, against predictions from earlier work on disk gap band parachutes[8,9] and subsonic wind tunnel tests of the test parachute[10]

The measured drag coefficient is plotted against the Mach number in Figure 12, alongside predictions from earlier work on disk gap band parachutes[8,9] and subsonic wind tunnel tests of the test parachute.[10] The numerical data fit well into the prediction bounds. There is a short data drop-out noticeable around Mach 0.41, due to a temporary saturation of the SD card bus. The agreement was very good between the speeds calculated from the pressure data and the speeds given by the GPS chip, despite the inflation speed being greater than the maximum speed quoted in the GPS chip specification.

The high-speed video footage of the inflation was disappointing, but can still show some aspects of the parachute inflation. A subsection of the frames are shown in Figure 13. During the high snatch loads the lens position moved inside the camera, causing blurring and zooming of the image. As the parachute lines became taut again the lens position moved further, increasing zoom markedly. With hindsight, the lens position would be fixed in the camera for future flights. Despite the poor focus, the rebounding of the parachute is clear to see in Figure 13(c-d).

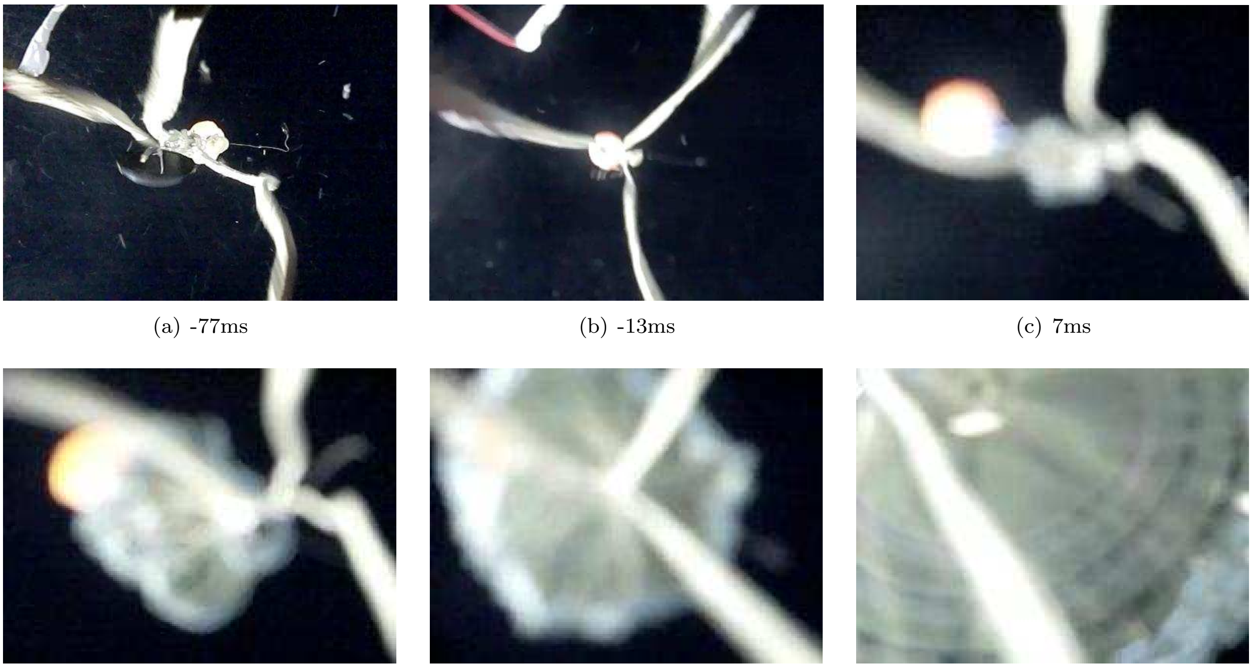

(a) -77ms (b) -13ms (c) 7ms

(d) 27ms (e) 47ms (f) 57ms

Figure 13. Inflation sequence at a velocity of 210.5m/s (Mach 0.71), an altitude of 22.2km ($72,800$ft) and an atmospheric density of 0.056kg/m^3. The initial snatch loads shift the lens position within the camera, causing the blurring between (b) and (c). The parachute then rebounds which can be seen from the slack lines in (c) and (d). When the parachute begins to decelerate the vehicle at ≈ 50g, the lens position changes again increasing the zoom sharply between (e) and (f).

VII. Conclusion

This paper describes a low-cost method for testing small parachutes (< 5m) at high Mach numbers in a low density environment. Wind tunnel facilities exist that can provide both high Mach number conditions and low densities, but they can only accommodate small scale parachutes in order to keep the tunnel blockage low. For larger parachutes, equivalent facilities do not exist, and would be prohibitively costly to run if they did. High-altitude tests can offer the conditions that wind-tunnels cannot.

Consumer electronics offer high accuracy sensors that can be used in a small, lightweight and low power instrumentation package. When combined with a small drop vehicle this allows for a significant reduction in launch complexity, as off-the-shelf latex weather balloons are sufficient to reach altitudes approaching 30km. Consumer high-speed cameras have advanced enough to be a cost-effective way of monitoring inflation characteristics, but the camera lens must be modified to have a fixed position or image focus may suffer during large decelerations.

For the vehicle designed in this paper, the per-launch expendable costs (balloon, helium etc.) are of the order of several thousand pounds (GBP). This provides an extremely cost effective way of testing small parachutes for stability and performance at the design Mach number and appropriate mass ratio. For a large planetary entry project, such a method could be a quick way of comparing initial designs, as a precursor to more expensive full scale tests. There is also scope to extend the vehicle design to include a rocket booster section, in order to evaluate inflation performance at supersonic Mach numbers. This would not significantly raise the per-launch cost of the vehicle.

Acknowledgments

This work was funded by the European Space Agency through Thales-Alenia Space Italy, the ExoMars prime contractor and Thales-Alenia Space France, the parachute system subcontractor. The authors also wish to thank BOC Speciality Gases, Cambridge Precision manufacturing, the Royal Aeronautical Society, Lesley Gore and Dr. Madsen Pirie for their continued support to the Cambridge University Spaceflight project.

References

[1]Murrow, H. N. and McFall Jr., J. C., *Some Test Results from the NASA Planetary Entry Parachute Program*, Journal of Spacecraft and Rockets, Vol. 6, No. 5, 1969, pp. 621-623.

[2]Stone, F. J., *Final Technical Report, 55-ft-D0 Ringsail Parachute, Planetary Entry Parachute Program*, NASA CR-66588, 1967.

[3]McFall, J. C. and Murrow Jr., H. N., *Parachute Testing at Altitudes Between 30 and 90 Kilometers*, Journal of Spacecraft and Rockets, Vol. 4, June, 1967, pp. 796-798.

[4]Eckstrom, C. V. and Preisser, J. S., *Flight Test of a 40-Foot-Nominal-Diameter Disk-Gap-Band Parachute Deployed at a Mach Number of 2.72 and a Dynamic Pressure of 9.7 Pounds per Square Foot*, NASA TM X-1623, 1968.

[5]Preisser, J. S. and Grow, R. B., *High-Altitude Flight Test of a Reefed 12.2-Meter-Diameter Disk-Gap-Band Parachute with Deployment at a Mach Number of 2.58*, NASA TN D-6469, 1971.

[6]Cruz, J. R. and Lingard, J. S., *Aerodynamic Decelerators for Planetary Exploration: Past, Present, and Future*, AIAA Guidance, Navigation, and Control Conference and Exhibit, AIAA 2006-6792, 2006.

[7]Mitcheltree, R., Bruno, R., Slimko, E., Baffes, C. and Konefat E., *High Altitude Test Program For A Mars Subsonic Parachute*, AIAA 18th Aerodynamic Decelerator Systems Technology Conference, AIAA-2005-1659, 2005.

[8]Underwood, J. C., *Development testing of Disk-Gap-Band parachutes for the Huygens probe*, Aerodynamic Decelerator Systems Technology Conference, 13th, Clearwater Beach, FL, AIAA-1995-1549, 1995.

[9]Underwood, J. C. and Sinclair, R., *Wind Tunnel Testing of Parachutes for the Huygens Probe*, CEAS, Cambridge, UK, 1997.

[10]Lingard et al., *ExoMars Parachute System*, Aerodynamic Decelerator Systems Technology Conference, 20th, Seattle, WA, AIAA 2009-2975, 2009.